Journal Pre-proofs

Machine vision-based non-destructive dissolution prediction of meloxicam-containing tablets

Lilla Alexandra Mészáros, Lajos Madarász, Szabina Kádár, Máté Ficzere, Attila Farkas, Zsombor Kristóf Nagy

PII: S0378-5173(24)00247-3
DOI: https://doi.org/10.1016/j.ijpharm.2024.124013
Reference: IJP 124013

To appear in: *International Journal of Pharmaceutics*

Received Date: 22 December 2023
Revised Date: 15 March 2024
Accepted Date: 15 March 2024

Please cite this article as: L. Alexandra Mészáros, L. Madarász, S. Kádár, M. Ficzere, A. Farkas, Z. Kristóf Nagy, Machine vision-based non-destructive dissolution prediction of meloxicam-containing tablets, *International Journal of Pharmaceutics* (2024), doi: https://doi.org/10.1016/j.ijpharm.2024.124013

Machine vision-based non-destructive dissolution prediction of meloxicam-containing tablets

Lilla Alexandra Mészáros[1], Lajos Madarász[1], Szabina Kádár[1], Máté Ficzere[1], Attila Farkas[1], Zsombor Kristóf Nagy[1]*

[1] Department of Organic Chemistry and Technology, Budapest University of Technology and Economics, H-1111 Budapest, Műegyetem rakpart 3, Hungary

*Corresponding author: zsknagy@oct.bme.hu; Phone: +36-1-463-4129

ABSTRACT

Machine vision systems have emerged for quality assessment of solid dosage forms in the pharmaceutical industry. These can offer a versatile tool for continuous manufacturing while supporting the framework of process analytical technology, quality-by-design, and real-time release testing. The aim of this work is to develop a digital UV/VIS imaging-based system for predicting the *in vitro* dissolution of meloxicam-containing tablets. The alteration of the dissolution profiles of the samples required different levels of the critical process parameters, including compression force, particle size and content of the API. These process parameters were predicted non-destructively by multivariate analysis of UV/VIS images taken from the tablets. The dissolution profile prediction was also executed using solely the image data and applying artificial neural networks. The prediction error (RMSE) of the dissolution profile points was less than 5%. The alteration of the API content directly affected the maximum concentrations observed at the end of the dissolution tests. This parameter was predicted with a relative error of less than 10% by PLS models that are based on the color components of UV and VIS images. In conclusion, this paper presents a modern, non-destructive PAT solution for real-time testing of the dissolution of tablets.

KEYWORDS

Dissolution prediction, Dissolution testing, Artificial neural network, Machine vision, Quality assessment, Meloxicam

1. Introduction

Regulatory agencies in the pharmaceutical sector prioritize innovation and continuous improvement to maintain quality, sustainability, efficiency and productivity [1][2]. In production processes these are critical and requiring manufacturers to stay up-to-date with constantly evolving requirements and the competition among industrial players [2].

The demand for the implementation of continuous manufacturing through process analytical technology (PAT) has increased in recent years owing to the numerous financial and environmental benefits [3]. This trend also promotes adopting process design and development based on the deep understanding of both the process and the product. Additionally, it facilitates

the implementation of the quality-by-design (QbD) approach. Thus, the main point of interest has become real-time, non-destructive, quality-based monitoring and control following the publication of the regulatory guidelines [4].

In the pharmaceutical market solid dosage forms are significantly represented, particularly tablets [5]. In the context of modernization, the development of new and innovative analytical systems and solutions for quality assessment remains a relevant area [6]. The QbD approach necessitates a thorough understanding, continuous monitoring, and control of critical quality attributes (CQAs) and critical process parameters (CPPs), such as compression force, hardness, content uniformity and *in vitro* dissolution behavior of tablets [7]. Traditionally, standardized in-process control tests are carried out during production, applying offline specialized equipment, often using destructive methods.

In vitro dissolution testing is an essentital procedure for assessing the *in vivo* effectiveness of the product. It is also applied during the research, development and manufacturing phases [8][9][10]. Despite being well understood and also required by regulatory agencies, this procedure is destructive, time-consuming, resulting in high resource demands and limitations on the number of samples that can be measured and evaluated [11][12][13]. The aleatory occurrence of variability in the profiles can be linked to several parameters, including the operator, the apparatus, and the tablet position in the vessel [10][8]. Moreover, the dissolution behavior significantly affected by various critical process parameters, leading to batch-to-batch variability [14]. These factors have driven attention to connect analytical science and manufacturing to achieve real-time *in vitro* dissolution predictions [12].

Near-infrared spectroscopy (NIRS) coupled with multivariate data analysis dominates the field of predictions of various CQAs and CPPs. This technique is a widely applied PAT tool and is supported by regulatory agencies [15][12]. The application of advanced data analysis methods, such as partial least squares and artificial neural networks (ANNs) was considered significant [12]. In their study, Freitas *et al.* utilized diffuse reflectance NIRS to establish a linear relationship between the NIR spectra of clonazepam tablets and their *in vitro* dissolution rate while varying the amounts of excipients [16]. Ojala *et al.* employed diffuse reflectance NIRS to predict the drug release from tablets containing toremifene as an API. The correlation between the drug release and the NIRS measurements was determined using PLS [14]. The application of artificial neural networks by Nagy *et al.* facilitated the prediction of the *in vitro* dissolution of caffeine-containing extended-release tablets using NIR and Raman spectroscopic data [12]. A PLS-2 model was created by Baranwal *et al.* utilizing NIRS data to anticipate the

dissolution profiles of multiple APIs in bilayer tablets [17]. The applicability of machine learning methods in predicting the *in vitro* dissolution of drotaverine-containing tablets was demonstrated by Galata *et al.* [18]. Beside NIRS tools, terahertz spectroscopy has also emerged as a valuable tool to provide modern solutions in the pharmaceutical industry [13]. Bawuah e*t al.* made predictions regarding the dissolution of immediate release tablets containing ibuprofen and indomethacin. These predictions were based on the porosity measurements obtained with terahertz spectroscopy [19].

Despite the extensive representation of these methods, the focus is also on the easily accessible and affordable sources of information and predictions [20]. In the recent years, machine vision has become increasingly important in the assessment of pharmaceutical quality [21]. These highly evolving systems and multivariate data analysis presents a cost-effective and real-time solution. This can serve as a PAT tool to facilitate the implementation of continuous manufacturing. These methods have already established their effectiveness in visual inspections to identify core or coating defects [15][22][23], digitalization processes of packaging and labels [24] and for process monitoring [25]. These highlight the adaptability and extensive applicability of machine vision in both in-process and end-product testing. However, the authors have not found any publications that discuss the implementation of a machine vision system in combination with multivariate data analysis for the purpose of predicting dissolution behavior of tablets.

The previous studies of the authors have introduced digital UV/VIS imaging-based methods for inspecting meloxicam-containing tablets. These methods were used to determine API content, compression force, crushing strength, particle size distribution of the API, and classify tablets with different particle sizes of the API, as well as map the API distribution. In that scenario, adjustments were made to one parameter at a time, and the resulting modifications were examined [26][27].

This study aims to establish a non-destructive, rapid, digital UV/VIS imaging-based machine vision method for predicting the altered *in vitro* dissolution of meloxicam-containing tablets. The alteration was carried out by simultaneously modifying the CPPs, which included adjusting the compression force, particle size distribution, and content of the API. Additionally, the objective was to examine the cumulative impact of these factors on the dissolution behavior of the samples. ANN-based prediction of the dissolution profiles relied on input data obtained from the particle size distributions of the API and the compression force values, both predicted by the developed UV/VIS imaging-based machine vision system. A correlation was established

between the color components of the images and the API content of the samples, indirectly influencing the dissolution rate. Consequently, the estimation of the maximum concentrations achieved during the dissolution tests was carried out using PLS models. The input dataset was comprised of the color components from images captured from the samples within the target range of compression force and particle size distribution. The performance of the developed models was also tested on an external dataset of meloxicam-containing tablets.

2. Materials and Methods

2.1. Materials

Meloxicam (MLX) was utilized as the active pharmaceutical ingredient (API), belonging to class 2 due to its high permeability and limited solubility in the Biopharmaceutics Classification System (BCS) [28]. Acetone, sodium hydroxide, and sodium-dihydrogen-phosphate were obtained from Sigma Aldrich (St. Louis, MO, USA). Vivapur 200 microcrystalline cellulose (MCC) was purchased from JRS Pharma (Rosenberg, Germany).

2.2. Methods

2.2.1. Preparation of the samples with altered *in vitro* dissolution behaviour

Particle size enlargement of the API by crystallization and the characterization of the product

In order to decrease the dissolution rate, the particle size of the API was increased compared to its initial size. For the particle size enlargement of MLX, slow cooling and evaporation method from the publication of Bolourchian et al. was used [29]. 1 g of MLX was dissolved in acetone solvent in a crystallization dish and MLX concentration was set at 0.45 w/v%. 50°C, 100 rpm stirring was applied until a clear solution was obtained. The solution was kept overnight at room temperature to evaporate the applied solvent. The particle size distribution of the prepared crystals was determined by laser diffraction using Malvern Mastersizer 2000 (Malvern

Panalytical, UK) [30]. A manual placement of 1 g of crystalline sample was carried out on the sample tray of the dispersion unit. The sample was guided into a sieve with bearings by the vibration of the tray, to ensure controlled sample flow and disintegration of any loose agglomerates. Compressed air was utilized to provide the sample flow and dispersion. The parameters for the applied standard operation procedure were as follows: the vibrational feed rate was set to 40%, the dispersive air pressure was set to 1 bar, and the measurement time was 30 seconds. Particle size analysis is based on the application of the Mie theory. The measurement range of this instrument spans from 100 nm to 2 mm [30]. The initial MLX was labeled as $MLX_{25\mu m}$, while the enlarged form was labeled as $MLX_{176\mu m}^{Acetone}$ in the following. With the crystallized and initial MLX, two groups were created based on the different particle sizes. For the third group $MLX_{25\mu m}$ and $MLX_{176\mu m}^{Acetone}$ were mixed with 50:50 ratio to produce the samples.

Preparation of tablets

After weighing the components, powder mixtures were manually homogenized for 10 minutes. A total of 172 tablets were manually produced using a Dott Bonapace CPR6 (Dott Bonapace, Italy) eccentric tablet press, within the compression force range of 5-15 kN, and with the API content ranging from 2.3-3.5 w/w% as stated in **Table 1.** The tablet press was equipped with a single concave punch. Biconvex tablets were obtained, with a diameter of 14 mm, weighing 400 ± 15 mg. The dissolution test results are highly affected by these parameters, along with the increased particle size. The application of higher compression force values also leads to an increase in the disintegration time of the samples. The model development utilized 135 tablets from the produced samples, while an additional 22 samples were used as an external dataset In order to predict the maximum concentration at the endpoint of the dissolution tests, an extended sample set was used in the calibration and validation process of the developed models.

Table 1. *The tablet properties and the experiment setup for predicting of in vitro dissolution behaviour*

Levels of particle sizes of API	Levels of compression force (kN)	Levels of nominal API content (w/w%)	Weight of powder mixture for each level	Number of samples
Sample set for model development				

$MLX_{25\mu m}$	5, 10,15	1.5, 2.5, 3.5	8g	1-45.
$MLX_{176\mu m}^{Acetone}$	5, 10,15	1.5, 2.5, 3.5	8g	45-90.
$MLX_{25\mu m}$+ $MLX_{176\mu m}^{Acetone}$	5, 10,15	1.5, 2.5, 3.5	8g	91-135.
Extended sample set used for model development				
$MLX_{25\mu m}$	10	1.5, 2.5, 3.5	3g	C1-15.
External test set used for the application of the developed models				
$MLX_{25\mu m}$	8, 10, 12	2.3, 2.5, 2.7	5g	1-2., 6-22.
$MLX_{176\mu m}^{Acetone}$	10	2.5		3-4.
$MLX_{25\mu m}$+ $MLX_{176\mu m}^{Acetone}$	10	2.5		4-5.

2.2.2. *In vitro* dissolution testing

The *in vitro* dissolution testing was conducted using the paddle method (US Pharmacopoeia II) on the Hanson SR8-Plus dissolution tester (Hanson Research, Chatworth, CA, USA). The dissolution medium consisting of a pH=6.8 phosphate buffer, and the volume of 900 ml. The applied temperature was maintained at 37 ± 0.5°C, while the paddle rotation speed was set to 100 rpm. Released API content was measured online at a wavelength of 363 nm using an online UV/VIS spectrophotometer (Hewlett-Packard, CA, USA). The time interval of the tests was 24 hours. In order to achieve a deeper comprehension and distinction between the dissolution profiles, a total of 70 sampling points were employed. Following the 2-minute and 5-minute sampling, the interval was modified to every 10 minutes until 190 minute. Subsequently, sampling periods of 20 and 30 minutes were implemented.

2.2.3. Image acquisition

The in-house production of the image acquisition layout was carried out by the authors and previously published [26]. This layout can be mounted above a conveyor belt. The image acquisition was performed using a Basler acA4112-30uc area scan camera (Basler, Germany), which incorporates a CMOS sensor. It was equipped with the Basler MEGA TS1214-MP objective (Basler, Germany). The illumination was provided by a ring light, which contains

three rows of white, light emitting diode (LED, VIS), or a UV ringlight, which consists of 6 ultraviolet LEDs, emitting light in the 380-395 nm range (UV) (Apokromat Ltd., Hungary). The exposition time for acquiring VIS images was set to 1200 μs, whereas for UV images it was set to 30000 μs. Both sides of the prepared samples were examined, resulting in images with dimensions of 480x480 pixels.

2.2.4. The algorithms utilized in the quality-based assessment, specifically for the *in vitro* dissolution of MLX-containing tablets

The applied algorithms were developed within the MATLAB R2020a environment (MathWorks, Natick, MA, USA). The PLS models were generated using PLS Toolbox 8.8.1 (Eigenvector, Manson, WA, USA). Wavelet-based analysis of the images was performed using Wavelet Toolbox 5.4 (MathWorks, Natick, MA, USA). The Deep Learning Toolbox 14.0 (MathWorks, Natick, MA, USA) was utilized for the tasks of neural network-based predictions and classifications. **Figure 1**. summarize the developed algorithms in a flowchart.

In order to create an appropriate dataset for profile prediction, it was necessary to gather information on the compression force and particle size distribution. Hence, these were estimated by applying the acquired VIS and UV images. The API content must be taken into consideration in order to accurately estimate the *in vitro* dissolution behavior. This parameter has the potential to influence the maximum dissolved content at the end of the tests and may be linked to the color components of the images acquired from the samples. The subsequent algorithms were utilized to predict these parameters for the dissolution-based evaluation of the prepared samples.

After importing the images, the background extraction process was uniformly implemented in all cases. In the initial step, the images were binarized, followed by the detection of circles with the determined radius using circular Hough-transformation.

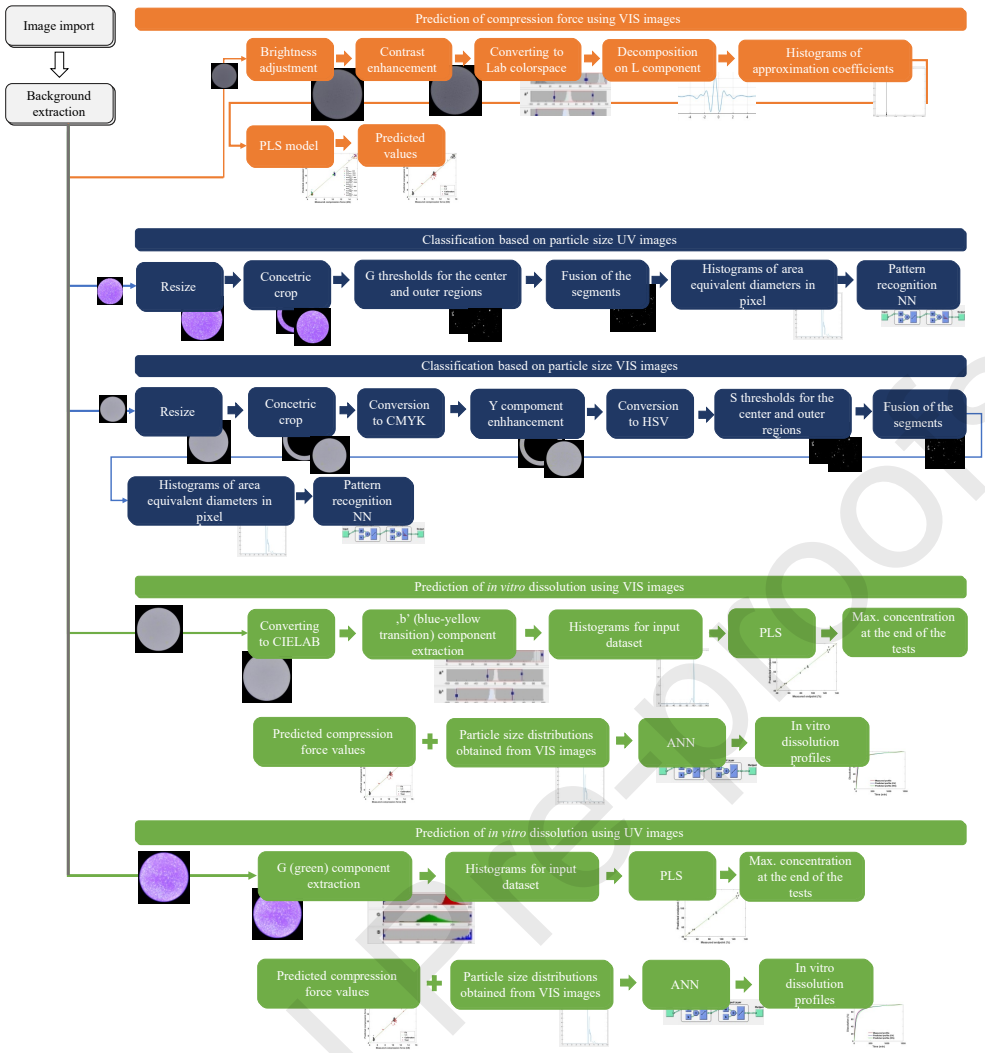

Figure 1. *The detailed presentation of developed algorithms for the prediction of compression force, particle size distribution, in vitro dissolution profile and the maximum concentration at the end of the tests*

Prediction of compression force

An algorithm was developed using wavelet-based analysis and VIS images for the prediction of compression force. The authors have previously demonstrated the successful application of the developed algorithm to MLX-containing tablets [26]. Taking into account the nature of the images and the requirement to highlight surface details, brightness adjustment and contrast enhancement were carried out after the background extraction. In the subsequent step, wavelet decomposition was performed on the monochromatic images based on the L component using Daubechies2 and Meyer wavelets. Histograms were generated using the approximation coefficients and applied as input dataset for PLS. Autoscale preprocessing and venetian blinds cross-validation were implemented with 10 splits in the development of the PLS model. To

assess the performance of the developed models, R^2CV (determination coefficient of cross-validation), RMSECV (root mean square error of cross-validation), RMSEP (root mean square error of prediction, and the number of latent variables (No. of LVs) were employed. The obtained performance parameters are presented in **Figure 6.**

Classification based on the particle size and the prediction of particle size distribution of the API

A two-step process was carried out to gather information on the particle size of the API. The methodology comprised the execution of permissive thresholding to enhance distinguishable regions on the surface, which was then followed by classification. Considering the determined classes, it is possible to apply stricter thresholds in order to predict the particle size distribution. Processing of VIS and UV images involved the application of two algorithms. Image resizing was achieved using the sophisticated Lanczos kernel mathematical approach. Due to the characteristics of the low-resolution UV images and the variations in critical parameters, concentric image cropping was necessary. Following that, the thresholds for the cropped images were determined utilizing the G (green) component from the RGB colorspace of the API containing regions. The fusion of the resulting binary images took place in the next step, followed by calculating the area equivalent diameters in pixels. The input dataset for the pattern recognition neural network (PRNN) was generated by creating histograms from the mentioned values. The determination of the target classes was based on the applied particle size groups of MLX.

Due to the specific characteristics of the VIS images, a slightly modified algorithm was employed for this purpose. Following the segmentation process, the images were transformed into the CMYK colorspace, mainly focusing on enhancing the Y (yellow) component to expose the API particles present on the surface. The CMYK images were converted to HSV colorspace. The determination of thresholds was carried out for the S (saturation) component. In the following steps, the center and outer region were combined through image fusion. The final steps remain unchanged as outlined in the algorithm for UV images.

The obtained datasets using the mentioned method based on UV and VIS images were applied as the input for PRNNs. The training, validation and test set ratio was 70:15:15. The elements of the sets were randomly selected. In feedforward network structure an input, a hidden and an output layer was utilized. The applied training function was scaled conjugate gradient

backpropagation. The output layer contained softmax transfer function. The optimization of neuron numbers was performed across a range of 1-15 neurons in all cases, with 100 instances of training. Each training process was restricted to a maximum duration of 20 epochs. The PRNNs was initialized with the default hyperparameters [31]. The results and goodness parameters were computed as an average. Target classes were based on the prepared API particles in different sizes, as mentioned in Section *2.2.1.* For evaluation of the performance of PRNNs, root mean square error (RMSE) and cross-entropy (CE) were applied. The performance is considered to be good when these values approximating zero.

In order to determine the particle size distribution of the API in the samples, more stringent thresholds were set for the various API groups based on the classifications derived from UV and VIS images. Particle size distributions were determined using area equivalent diameters, which were converted from pixels to microns using the QPCard 101 v3 millimeter reference scale (Argraph Corp., NJ, USA). The comparison between the measured and the predicted distributions was conducted using metric. When the value of the Wasserstein distance approximates zero, two distributions were considered similar.

In vitro dissolution prediction of the prepared tablets

The *in vitro* dissolution profile predictions were executed using ANNs. For this purpose, the dissolution curves were normalized between the 0-100% range of the dissolution rate. The compression force values and the particle size distributions, both obtained using the machine vision system, were applied as the inputs of the ANNs. The applied feedforward ANNs consisted of three layers: an input layer, a hidden layer, and an output layer. The training and validation set contained 70% and the test set contained the remaining 30% of the samples. The elements of the sets were selected randomly. The used training function was Bayesian regularization [32]. In order to prevent overfitting a training process with maximum of 7 epochs were utilized. The default hyperparameters of the ANN were implemented [32]. The optimization occurred in a similar manner as mentioned in the context of PRNNs for classification. RMSE values were also utilized to assess the performance of the ANNs. The predicted and measured profiles were compared using f2 (similarity) factor using DDSolver [33].

The color components of UV and VIS images were utilized to predict the maximum API release obtained from the measured dissolution curve in the last sampling, referred to as maximum concentration thereafter. Following the background extraction steps, the G (green) components

were extracted from the UV images in the RGB color space. Histograms were generated from these values, which constituted the input dataset for the PLS. The calibration process involved the application of autoscale preprocessing and venetian blinds cross-validation with 10 splits. The VIS images underwent a conversion from RGB to CIELAB colorspace. Based on the color of the API, the 'b' (blue-yellow transition) component was applied. The subsequent steps were identical to those mentioned for UV images. In order to evaluate the performance of the developed models, the same parameters were utilized as mentioned in the case of predicting compression force. The obtained values are presented in **Figure 13.**

3. Results and Discussion

3.1. Acquired images of the samples and the comparison of the surfaces under altered attributes

The acquired images of the prepared tablets are shown in **Figures 2-4**.

Altering the particle size of MLX and the compression force has a dual effect, not only on the dissolution rate but also on the visual properties of the surface (**Figure 2**). The utilization of UV and VIS light sources allows for the differentiation of API particles from the MCC matrix based on the acquired images. In the case of $MLX_{25\mu m}$, the naked eye could discern the individual particles in the UV images, but the utilization of VIS images will require advanced image preprocessing to enhance the visibility of these small particles. The examination of the $MLX_{176\mu m}^{Acetone}$ particles utilizing UV or VIS sources can be easily conducted whether they are applied individually or incorporated into a mixture with $MLX_{25\mu m}$. Accordingly, changes in the particle size can be identified on the surface of the samples. However, the application of UV illumination contributed to more significant effect. Based on these findings, the images provide sufficient information to determine or classify tablets based on particle size. Because of the low resolution, the diameters of the samples were estimated to be around 380 in pixels.

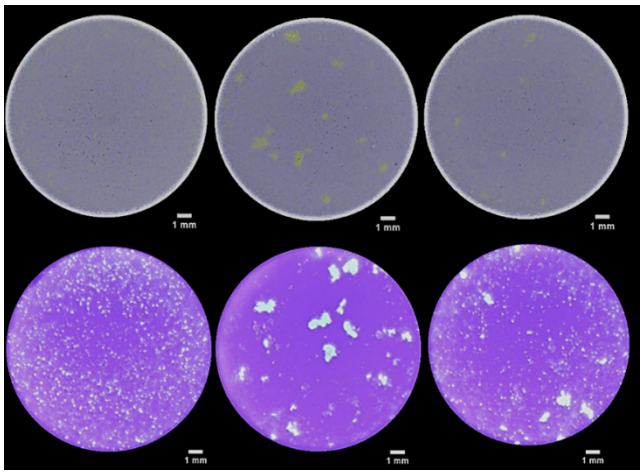

Figure 2. *The acquired, contrast enhanced VIS (first row) and UV (second row) images of three prepared tablets produced at 10 kN compression force and 1.5 w/w% API content with varying particle sizes (from left to right:* $MLX_{25\mu m}$, $MLX_{176\mu m}^{Acetone}$, $MLX_{25\mu m}$ + $MLX_{176\mu m}^{Acetone}$ *containing tablets)*

VIS images of the samples exhibit visible changes that correspond to the applied compression force, even at low resolution (**Figure 3**). This offers the potential for predicting attributes like compression force and crushing strength, which rely on the surface structure. Notably, observing this phenomenon in UV images of this resolution was impossible. The variations in compression force can also result in subtle changes in color on the surface, particularly along the concentric edges of the samples. This could be seen in both VIS and UV images in this resolution. Consequently, this aspect is important to take into consideration as it has the potential impact on the determination of API content or maximum concentration of the dissolution test. The influence of this parameter on the concentric edges of the tablets is minimal in relation to particle size prediction. This phenomenon is caused by the biconvexity of the samples.

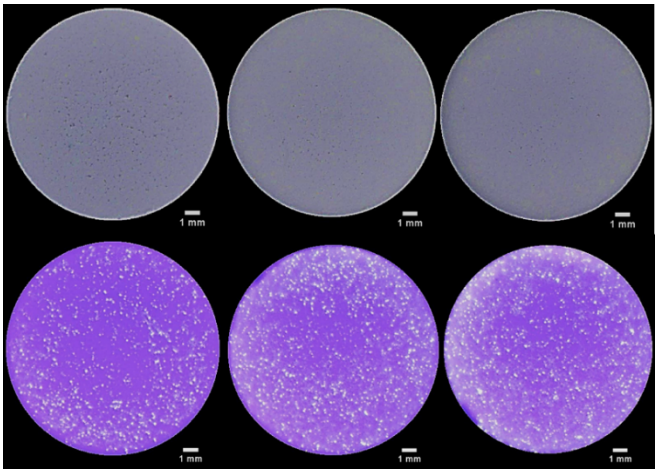

Figure 3. *The acquired, contrast enhanced VIS (first row) and UV (second row) images of three prepared 2.5 w/w%,* $MLX_{25\mu m}$ *containing tablets with varying compression force (from left to right: 5 kN, 10 kN, 15 kN)*

The changes in surface color could be indicative of a correlation with the API content or with the maximum concentration obtained from the dissolution tests in the applied range (**Figure 4**). It is visually represented with a saturated yellow hue in VIS images. This effect became more pronounced in UV images as the content increases. An increased quantity of particles was observed on the surface of the samples, resulting in a more noticeable color change from blue to yellow. This phenomenon is also observed when a larger particle size of the API was applied. Despite this, the concentric edge of the sample is affected by the increasing MLX content.

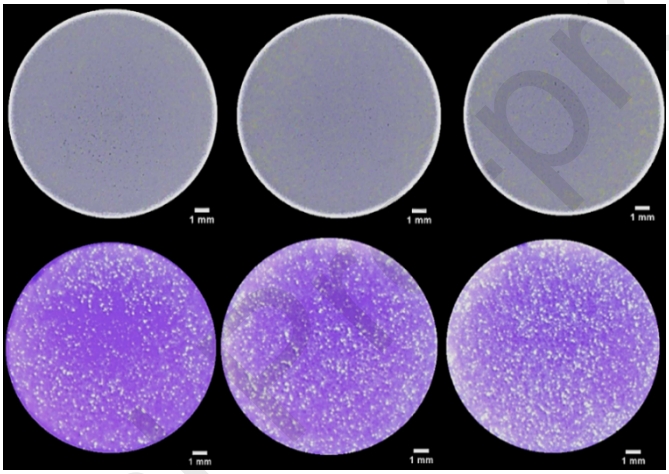

Figure 4. *The acquired, contrast enhanced VIS (first row) and UV (second row) images of three prepared* $MLX_{25\mu m}$ *containing tablets using 10 kN compression force with varying API content (from left to right:1.5 w/w%, 2.5 w/w%, 3.5 w/w%)*

3.2. The results of the *in vitro* dissolution tests of the produced samples

In vitro dissolution tests were conducted on a total of 157 samples. This sample set contained five samples from each combination of the levels of the mentioned CPPs. The dataset provided a suitable size for testing the capabilities of image analysis and neural networks in predicting altered profiles. The results of the tests were presented in **Figure 5.**

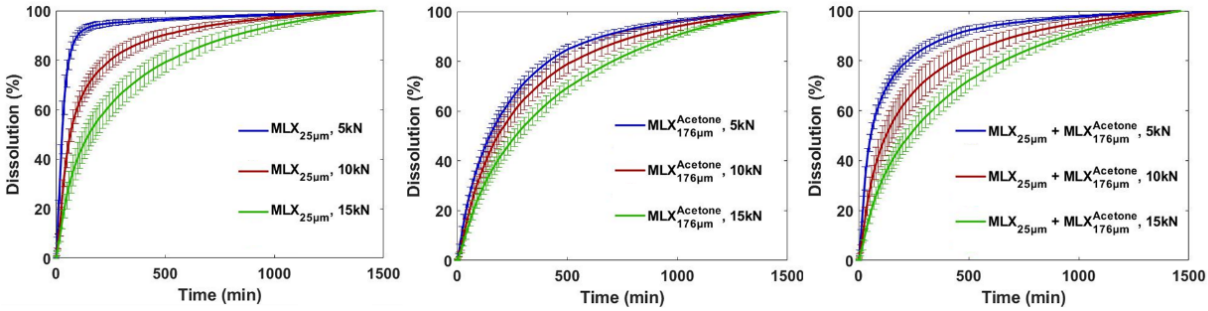

Figure 5. *The in vitro dissolution profiles of MLX-containing tablets using different particle size groups and compression force levels*

Figure 5 shows that as the particle size of the API increases, the dissolution rate highly decreases. Based on the visual inspection of the images obtained from the samples and the analysis of the dissolution profiles, it can be determined that the alteration was successful.

However, when examining the dissolution profiles at different particle size levels, only the compression force that determines the profiles. The profiles can be differentiated at the applied compression force levels of 5, 10, and 15 kN, with the dissolution rate decreasing as the levels increase. In summary, both examined parameters in the applied range exhibit an impact on the rate of dissolution. Thus, it is crucial to understand the impact of these important factors for proper *in vitro* dissolution prediction.

3.3. Creating a comprehensive dataset for *in vitro* dissolution profile prediction

3.3.1. Prediction of compression force

Based on the visual inspection of the images taken from the samples, it is possible to gather information regarding the compression force. After the development of the model, this parameter was quantitatively estimated to generate the input dataset for *in vitro* dissolution prediction.

Model development

A model was developed to predict compression force using a dataset of 135 samples. The samples were selected randomly, with 70% allocated for the calibration set and 30% allocated for the validation set. Previous research by the authors confirmed the feasibility of predicting the mentioned parameter on VIS images of meloxicam-containing tablets by solely altering this

parameter. Nevertheless, in this case, the compression force, along with the API content and the particle size of the API, were changed. The PLS model and the goodness parameters for the calibration and validation are presented in **Figure 6 a)** and **b)**.

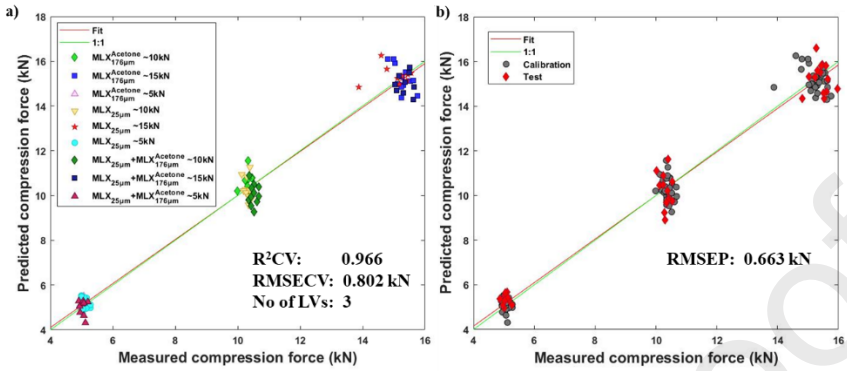

Figure 6. *a) The obtained PLS model and the goodness parameters for calibration, b) the results of the model validation and the obtained RMSEP value*

During the model development stage for compression force, the PLS model accurately predicted this parameter with a relative error of 7.74% for the median of the applied range. The approval limit for this value is $\pm$ 10% and it falls within that range. In comparison to the model previously obtained by the authors, only the changes in compression force showed similar goodness (RMSEP: 0.836 kN) and relative error (6.8%) values. This indicates that the algorithm and compression force prediction method, utilizing the acquired VIS images, can be successfully used for model development in scenarios where critical parameters are subject to change.

Application of the model for samples of the external test set

The model obtained for predicting compression force was applied to an external test set to simulate its application and assess its performance. The predicted values for the mentioned dataset were displayed with the calibration set in **Figure 7**. The relative error in the median of the test set was 8.26%. Accordingly, the obtained model was successfully applicable to an external dataset of MLX containing samples.

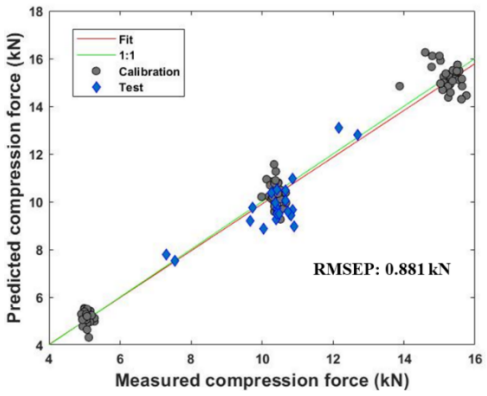

Figure 7. *Obtained result of compression force prediction for the external dataset displayed with the calibration set*

There are slight variances that can be observed between the predicted and measured values. According to **Table 2** samples labeled as 3-6, in which $MLX_{176\mu m}^{Acetone}$ and $MLX_{25\mu m}$ were applied, exhibit lower values than measured. It is important to emphasize that a single model has the ability to predict the compression force under the condition where multiple parameters undergo simultaneous changes. The target compression force was 10 kN, which was determined by the authors. The dissolution profiles of Samples 1-2 and 15-16 are expected to be greatly influenced by the compression force, based on the predicted values. The measured values also provided support for this observation (**Figure 14**).

Table 2. *The measured and the predicted compression force values of the samples from the external test set*

No. of sample	Measured value	Predicted value	No. of sample	Measured value	Predicted value
1	12.2 kN	13.1 kN	12	10.9 kN	11.0 kN
2	12.7 kN	12.8 kN	13	9.7 kN	9.2 kN
3	10.4 kN	9.7 kN	14	9.7 kN	9.8 kN
4	10.4 kN	9.3 kN	15	7.6 kN	7.6 kN
5	10.9 kN	9.0 kN	16	7.3 kN	7.8 kN
6	10.9 kN	9.7 kN	17	10.1 kN	8.9 kN
7	10.8 kN	9.5 kN	18	10.3 kN	10.4 kN
8	10.7 kN	10.5 kN	19	10.4 kN	10.5 kN
9	10.4 kN	11.0 kN	20	10.3 kN	9.9 kN
10	10.8 kN	9.2 kN	21	10.7 kN	9.6 kN
11	10.7 kN	10.1 kN	22	10.4 kN	9.5 kN

To summarize, the obtained model and results for the test set suggest the possibility of predicting the compression force of MLX-containing tablets using VIS images, even in the presence of variations in multiple critical parameters, such as the API content and particle size. The predicted compression force values provide a compact and manageable dataset suitable for input into subsequent models.

3.3.2. Prediction of the particle size of the API

The measured dissolution curves confirmed the importance of predicting the particle size of the API. This prediction was carried out using a method that combined qualitative and quantitative analysis.

Model development for qualitative analysis of particle size

The classification based on the produced three different particle sizes of the API was carried out using both UV and VIS images. These tasks were executed by applying PRNNs. 135 tablets were divided in a proportion of 70:15:15 for training, validation, and testing purposes. The use of a random partition of the input dataset led to a minor skew in the distribution of particle size groups among the training, validation, and test sets. The neural networks underwent optimization through training with 100 iterations using a range of 1-15 neurons. **Figure 8** provides a summary of the misclassified sample ratio in the test set during the optimization process for UV and VIS imaging-based input datasets. The obtained values led to the selection of 14 and 15 neurons in the hidden layer for UV and VIS images.

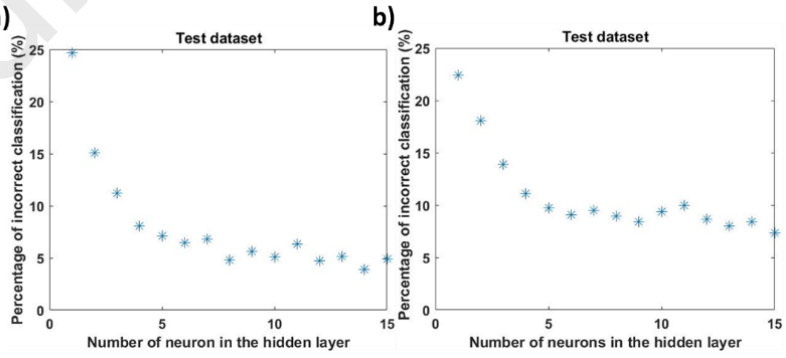

Figure 8. *The ratio of incorrect classification in the test set during the optimization of pattern recognition neural networks for classification based on the particle size (a) using UV and (b) using VIS images*

The neural networks were able to establish a correlation between the applied images and the particle sizes, as demonstrated in **Table 3**, which displays the CE and the average RMSE values. These values indicate the trained PRNNs' effective performance in the classification tasks. The values of both the RMSE and CE have been obtained at a small value.

Table 3. *The summary of the goodness parameters of the applied pattern recognition neural networks*

Image type	Dataset	RMSE	CE	Incorrect classification	Correct classification
UV	Training	8.93×10^{-2}	2.21×10^{-2}	1.1%	98.9%
	Validation	1.17×10^{-1}	3.43×10^{-2}	0%	100%
	Test	1.25×10^{-1}	3.86×10^{-2}	0%	100%
VIS	Training	1.09×10^{-1}	3.36×10^{-2}	2.1%	97.9%
	Validation	1.77×10^{-1}	6.54×10^{-2}	0%	100%
	Test	1.85×10^{-1}	7.22×10^{-2}	0%	100%

Pattern recognition neural networks reliably classified the prepared samples using information from the images, as shown by the confusion matrices (**Figure 9**). Only one was misclassified out of the UV illuminated images in the training set. In contrast, two images in the training set were misclassified using VIS images. All the samples were correctly classified during testing and validation. The slight imbalance in the ratio of the particle size classes within the sets did not present any limitations on the execution of the classification task. It is important to highlight that the classification results also produce a subset of samples where the dissolution profiles are affected by this critical parameter.

Figure 9. *The confusion matrixes for training, validation, and test sets for VIS (first row) and UV (second row) images (1. group: $MLX_{25\mu m}$, 2. group: $MLX_{176\mu m}^{Acetone}$, 3. group: $MLX_{176\mu m}^{Acetone}$ + $MLX_{25\mu m}$)*

Application of trained pattern recognition neural networks for classification of the samples from the external dataset

The PRNNs were applied using the same external sample set as mentioned in the prediction of compression force to assess the performance. The obtained confusion matrixes are shown in **Figure 10** for VIS and UV images.

Figure 10. *The confusion matrixes for external test sets for VIS (a) and UV (b) images (1. group: $MLX_{25\mu m}$, 2. group: $MLX_{176\mu m}^{Acetone}$, 3. group: $MLX_{176\mu m}^{Acetone}$ + $MLX_{25\mu m}$)*

The classification task was successfully executed using the developed algorithms and trained PRNNs, as indicated by the obtained confusion matrices. There were no occurrences of misclassified samples in the external test set. For UV images, the RMSE and CE values were 1.25×10^{-1} and 3.00×10^{-2}, respectively. For VIS images, the corresponding values were 4.65×10^{-2} and 1.54×10^{-2}. The classification was executed successfully on the samples of the external test set, as the obtained RMSE and the CE values were considered low.

Prediction of the particle size based on the results of the classification

Following the classification, an opportunity arose to assess the particle size distribution of the API in the prepared samples by employing more stringent thresholds of the color components. **Figure 11** displays the measured and obtained PSDs by applying all the samples from the determined groups. The limited resolution of the images restricts the ability to observe the complete range of the reference particle size analysis, particularly within the 2-20 μm interval. However, the domain size of these groups can be measured. As the alteration of the dissolution profiles was linked to the enlargement of the initial MLX, the significance of the mentioned interval was limited. Nevertheless the primary goal of this analysis was to discern the changes and collect data on the employed particle sizes of MLX. Hence, the resulting distributions can be utilized. The predicted distributions closely resembled those measured using laser diffraction method beside of the mentioned range. In the context of comparing the measured and the predicted distributions using the two illuminations, Wasserstein distances were calculated. The obtained higher values were caused by the limited resolution of the images. Based on these values it can be concluded that similar distributions can be obtained with both of the applied illuminations. Consequently, these particle size distributions were utilized as input for the subsequent analysis.

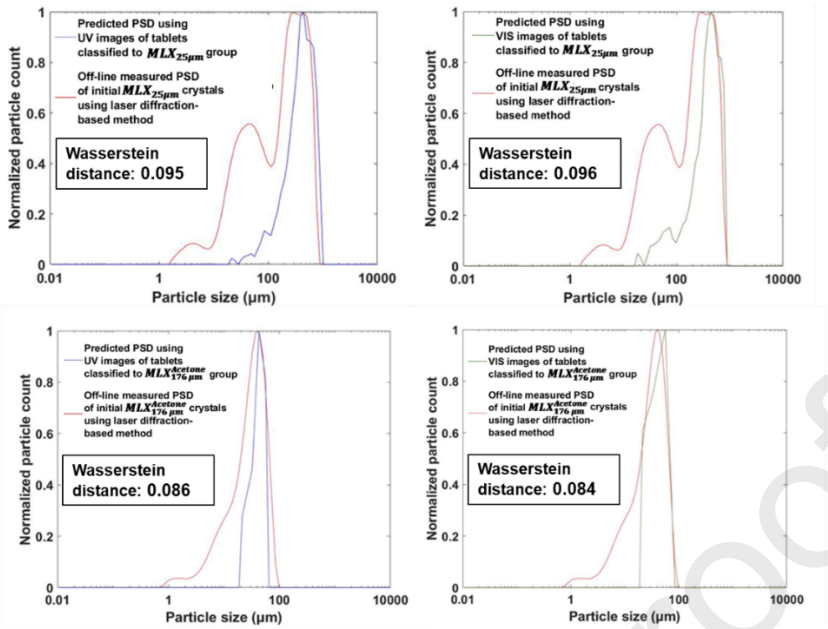

Figure 11. *The measured and the predicted PSDs of* $MLX^{Acetone}_{176\mu m}$ *and* $MLX_{25\mu m}$ *groups using UV (first column) and VIS (second column) images*

To conclude, the developed algorithms and the utilization of low-resolution images enable the execution of particle size determination, despite variations in compression force and API content within the applied range.

3.4. *In vitro* dissolution prediction

Model development for in vitro dissolution profile prediction

The input dataset included the predicted compression force and particle size distributions of the API. Both UV and VIS images were used to predict the profiles. The optimization of the networks can be observed in **Figure 12**. The selection of neuron numbers was determined by analyzing the square root of the performance function (MSE) obtained from the optimization process. Consequently, 14 and 15 neurons were chosen in the hidden layer.

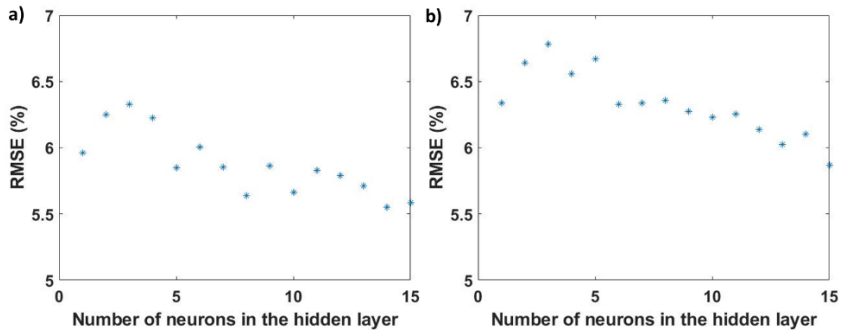

Figure 12. *The results obtained from optimizing neural networks to predict in vitro dissolution profiles using UV (a) and VIS (b) images*

In **Table 4**, the goodness parameters are presented, with a focus on the averaged RMSE values for the training and test sets based on one hundred runs. These percentages for the datasets were below 5%. The obtained results indicate that the application of the developed image processing algorithms and artificial neural networks can be utilized for predicting the mentioned parameter. The application of two distinct wavelengths of light yielded similar goodness. In addition, the simultaneous changes in particle sizes and compression force can be effectively managed by a single model.

Table 4. *The goodness parameter of in vitro dissolution profile predictions using UV and VIS images*

Image type	Dataset	RMSE	Image type	Dataset	RMSE
UV	Training	3.74%	VIS	Training	4.48%
	Test	4.24%		Test	4.59%

Taking the API content into consideration is vital for a proper *in vitro* dissolution prediction. Therefore, the predicted percentage of the API dissolved at the final sampling point is related to the mentioned parameter. The obtained images reveal that the prediction of compression force and particle size is achievable, and there is a connection between color change and API content. Therefore, this allows for the prediction of the maximum concentration of the dissolution test. For this purpose, a subset of samples within the target range were chosen from the total of 135. This corresponded to a total of 15 samples, which was further supplemented with an additional 15 samples from the extended set to construct a suitable dataset for model development. After splitting, 21 samples were used for calibration, and 9 samples for validation,

employing both VIS and UV images. The results and goodness parameters of the obtained PLS models are displayed in **Figure 13**.

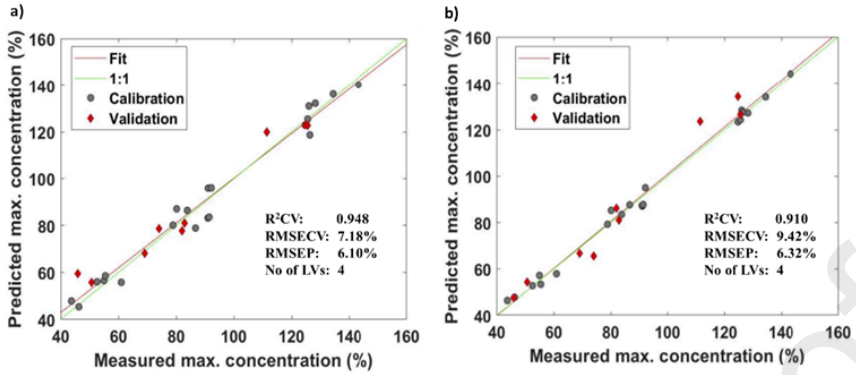

Figure 13. *The goodness parameters and the result of the calibration of PLS model in maximum concentration prediction for the dissolution tests based on UV (a) and VIS (b) images*

The goodness parameters of the maximum concentration predictions demonstrated similarity in both UV and VIS images. According to the values of R^2CV, RMSECV and RMSEP, the models were considered acceptable.

Application of the developed models for the prediction of dissolution profile and the maximum concentration of the in vitro dissolution tests for the external dataset

The demonstration of the application and evaluation of the trained ANNs utilized 22 samples of the external dataset. **Figure 14** summarize the measured and the UV and VIS images-based predictions with the f2 values. The RMSE values were 3.93% and 4.15% for using UV and VIS images, respectively.

Figure 14. *The measured (red) and the predicted profiles for the prepared tablet along with the f2 values using UV (blue) and VIS (green) images*

The average f2 values were 77.04 for UV images and 76.37 for VIS images. The performance of both ANNs was found to be similar. This outcome was anticipated in light of the particle size distribution and the compression force predictions. In conclusion, the algorithms and ANNs were successfully applied to predict the *in vitro* dissolution profile of MLX tablets produced within the specified range of compression force and particle size.

The prediction of the maximum concentration results for the 14 samples of the external test set and RMSEP values are displayed in **Figure 15** for both types of images. Considering these

values, the implementation of the PLS models were suitable, if a single parameter, the API content undergoes alteration through VIS or UV images.

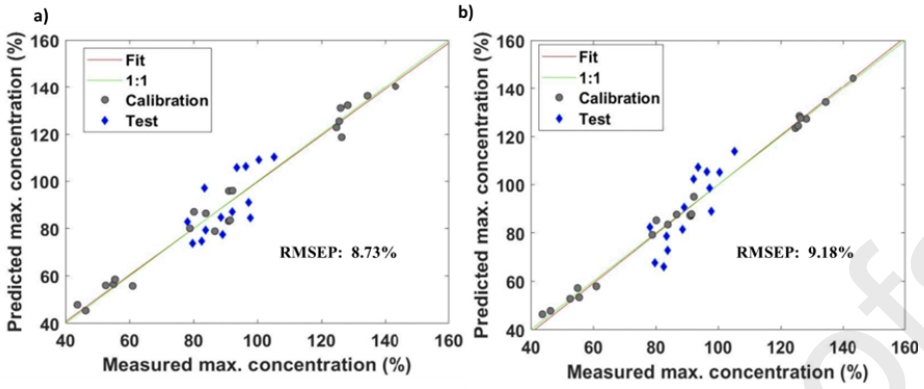

Figure 15. *The result of the maximum concentration prediction for the samples of external dataset based on UV (a) and VIS (b) images*

According to the RMSEP values obtained for the external dataset, the prediction can be carried out with a relative error of less than 10% for the target (USP limit for drug content error in a tablet is ± 25%). The *in vitro* dissolution behavior of the samples can be assessed by taking into account the predictions of the profiles and the maximum concentration. Various standard analytical methods can be applied to predict the API content. However, the primary advantage of machine vision its ability to provide information for each individual sample non-destructively on the production line. Moreover, the obtained models and predictions for the critical attributes can provide an opportunity to identify samples that did not meet the required quality.

4. Conclusion

In the pharmaceutical industry, modernization, innovation, and digitalization are at the center of attention. There is also an increasing interest in the utilization of machine vision systems as PAT tools. These methods can offer a rapid and non-destructive solution for evaluating the quality of solid dosage forms.

The dissolution characteristics of the prepared samples were modified by changing the particle size of the API, API content and compression force. The dataset used for *in vitro* dissolution profile prediction was generated through the utilization of imaging-based prediction of compression force and particle size. The presented work demonstrated that these sample attributes are successfully predictable even other critical parameters change at the same time.

In that scenario, the compression force was predicted utilizing VIS images, resulting in a relative error of 7.4%. The qualitative and quantitative assessment of the samples based on the particle size of the API can be executed even when low-resolution images are applied. The predicted and the measured particle size distributions showed a high similarity. In the context of *in vitro* dissolution prediction RMSEP values were less than 5%, and the averaged f2 similarity factors were 77, respectively. For the maximum concentration prediction the RMSEP valu-es were lower than 9%.

The prediction of compression force using VIS images is not reliant on the applied API or color; instead, it solely relies on the surface texture. Therefore, it could be possible to implement the algorithms and methods for other samples. The API color is particularly relevant when VIS images are employed to predict the maximal concentration of *in vitro* dissolution and analyze particle size. Therefore, the API can be evaluated through VIS images, in which the color or hue differs from the matrix component. It is crucial to acknowledge that the use of UV illumination can greatly expand the range of accessible colored or white APIs for evaluation. The importance of this arises when the API can be discriminated from the matrix component due to differences in color or hue. Therefore, the UV/VIS imaging-based system presented here has the capability to adapt to white APIs as well.

Based on the obtained results, there is a possibility of incorporating imaging to support complex quality assessment in the context of critical parameters, which is considered a crucial element in modern manufacturing. The characteristics of the developed system could fulfill the requirements of PAT and has the potential to contribute to QbD and RTRT approaches in the future. It should be noted that it can support the conventional methods used in that field by providing more information of the product. Moreover, the imaging-based system can enable the evaluation and selection of each sample based on the requirements. In conclusion the developed system could be a promising solution for predictions of critical attributes and can be utilized for a comprehensive quality assessment of MLX-containing tablets.

Acknowledgements

Supported by the ÚNKP-23-3-II-BME-88 and ÚNKP-23-4-I-BME-61 New National Excellence Program of the Ministry for Culture and Innovation from the source of the National Research, Development and Innovation Fund. Project no. RRF-2.3.1-21-2022-00015 has been implemented with the support provided by the European Union. This work was supported by OTKA grant FK-132133.

REFERENCES

[1] S. Šašić, *Innovations in Pharmaceutical Manufacturing on the Horizon: Technical Challenges, Regulatory Issues, and Recommendations*. Washington, D.C.: National Academies Press, 2021. doi: 10.17226/26009.

[2] J. Weitzel *et al.*, "Understanding Quality Paradigm Shifts in the Evolving Pharmaceutical Landscape: Perspectives from the USP Quality Advisory Group," *AAPS J.*, vol. 23, no. 6, pp. 1–8, Oct. 2021, doi: 10.1208/S12248-021-00634-5/METRICS.

[3] Y. Roggo, M. Jelsch, P. Heger, S. Ensslin, and M. Krumme, "Deep learning for continuous manufacturing of pharmaceutical solid dosage form," *Eur. J. Pharm. Biopharm.*, vol. 153, pp. 95–105, Aug. 2020, doi: 10.1016/J.EJPB.2020.06.002.

[4] J. Wahlich, "Review: Continuous Manufacturing of Small Molecule Solid Oral Dosage Forms," *Pharmacutics*, vol. 13 (8), 2021, doi: 10.3390/pharmaceutics13081311.

[5] Q. Zeng *et al.*, "Research progress on the application of spectral imaging technology in pharmaceutical tablet analysis," *Int. J. Pharm.*, vol. 625, Sep. 2022, doi: 10.1016/J.IJPHARM.2022.122100.

[6] N. Zaborenko *et al.*, "First-Principles and Empirical Approaches to Predicting In Vitro Dissolution for Pharmaceutical Formulation and Process Development and for Product Release Testing," *AAPS J.*, vol. 21, no. 3, May 2019, doi: 10.1208/S12248-019-0297-Y.

[7] U.S. Department of Health and Human Services, Food and Drug Adminitsration, and Center for Drug Evaluation and Research, "Dissolution Testing and Acceptance Criteria for Immediate-Release Solid Oral Dosage Form Drug Products Containing High Solubility Drug Substances Guidance for Industry," *Off. Commun. Div. Drug Inf. Cent. Drug Eval. Res.*, 2018, Accessed: Jan. 11, 2022. [Online]. Available: https://www.fda.gov/files/drugs/published/Dissolution-Testing-and-Acceptance-Criteria-for-Immediate-Release-Solid-Oral-Dosage-Form-Drug-Products-Containing-High-Solubility-Drug-Substances-Guidance-for-Industry.pdf

[8] E. Hernandez *et al.*, "Prediction of dissolution profiles by non-destructive near infrared spectroscopy in tablets subjected to different levels of strain.," *J. Pharm. Biomed. Anal.*, vol. 117, pp. 568–576, Jan. 2016, doi: 10.1016/J.JPBA.2015.10.012.

[9] S. Tabasi, V. Moolchandani, R. Fahmy, and S. Hoag, "Sustained release dosage forms dissolution behavior prediction: a study of matrix tablets using NIR spectroscopy," *Int. J. Pharm.*, vol. 382, no. 1–2, pp. 1–6, Aug. 2009, doi: 10.1016/J.IJPHARM.2009.07.029.

[10] Y. Zhao *et al.*, "Prediction of Dissolution Profiles From Process Parameters, Formulation, and Spectroscopic Measurements," *J. Pharm. Sci.*, vol. 108, no. 6, pp. 2119–2127, Jun. 2019, doi: 10.1016/J.XPHS.2019.01.023.

[11] P. Pawar, Y. Wang, G. Keyvan, G. Callegari, A. Cuitino, and F. Muzzio, "Enabling real time release testing by NIR prediction of dissolution of tablets made by continuous direct compression (CDC)," *Int. J. Pharm.*, vol. 512, no. 1, pp. 96–107, Oct. 2016, doi: 10.1016/J.IJPHARM.2016.08.033.

[12] B. Nagy *et al.*, "Application of artificial neural networks for Process Analytical Technology-based dissolution testing," *Int. J. Pharm.*, vol. 567, Aug. 2019, doi: 10.1016/J.IJPHARM.2019.118464.

[13] P. Bawuah *et al.*, "A Fast and Non-destructive Terahertz Dissolution Assay for Immediate Release Tablets," *J. Pharm. Sci.*, vol. 110, no. 5, pp. 2083–2092, May 2021, doi: 10.1016/J.XPHS.2020.11.041.

[14] K. Ojala, M. Myrskyranta, A. Liimatainen, H. Kortejärvi, and A. Juppo, "Prediction of drug dissolution from Toremifene 80 mg tablets by NIR spectroscopy," *Int. J. Pharm.*, vol. 577, p. 119028, Mar. 2020, doi: 10.1016/J.IJPHARM.2020.119028.

[15] C. Gendre, M. Boiret, M. Genty, P. Chaminade, and J. M. Pean, "Real-time predictions of drug release and end point detection of a coating operation by in-line near infrared measurements," *Int. J. Pharm.*, vol. 421, no. 2, pp. 237–243, Oct. 2011, doi: 10.1016/J.IJPHARM.2011.09.036.

[16] M. P. Freitas *et al.*, "Prediction of drug dissolution profiles from tablets using NIR diffuse reflectance spectroscopy: a rapid and nondestructive method," *J. Pharm. Biomed. Anal.*, vol. 39, no. 1–2, pp. 17–21, Sep. 2005, doi: 10.1016/J.JPBA.2005.03.023.

[17] Y. Baranwal *et al.*, "Prediction of dissolution profiles by non-destructive NIR spectroscopy in bilayer tablets," *Int. J. Pharm.*, vol. 565, pp. 419–436, Jun. 2019, doi: 10.1016/J.IJPHARM.2019.05.022.

[18] D. L. Galata *et al.*, "Real-time release testing of dissolution based on surrogate models developed by machine learning algorithms using NIR spectra, compression force and particle size distribution as input data," *Int. J. Pharm.*, vol. 597, p. 120338, Mar. 2021, doi: 10.1016/J.IJPHARM.2021.120338.

[19] P. Bawuah *et al.*, "Terahertz-Based Porosity Measurement of Pharmaceutical Tablets: a Tutorial," *J. Infrared, Millimeter, Terahertz Waves*, vol. 41, pp. 450–469, 2020, doi: 10.1007/s10762-019-00659-0.

[20] A. Ramadan, E. B. Basalious, and M. Abdallah, "Industrial application of QbD and NIR

chemometric models in quality improvement of immediate release tablets," *Saudi Pharm. J.*, vol. 29, no. 6, pp. 516–526, 2021, doi: 10.1016/j.jsps.2021.04.012.

[21] D. L. Galata *et al.*, "Applications of machine vision in pharmaceutical technology: A review," *Eur. J. Pharm. Sci.*, vol. 159, Apr. 2021, doi: 10.1016/J.EJPS.2021.105717.

[22] C. P. Rodrigues, C. Duchesne, É. Poulin, and P.-P. Lapointe-Garant, "In-line cosmetic end-point detection of batch coating processes for colored tablets using multivariate image analysis," *Int. J. Pharm.*, vol. 606, p. 120953, 2021, doi: 10.1016/J.IJPHARM.2021.120953.

[23] Y. Hou *et al.*, "A feasibility research on the application of machine vision technology in appearance quality inspection of Xuesaitong dropping pills," *Spectrochim. Acta Part A Mol. Biomol. Spectrosc.*, vol. 258, p. 119787, Sep. 2021, doi: 10.1016/J.SAA.2021.119787.

[24] M. Singh, S. Sachan, A. Singh, and K. K. Singh, "Internet of Things in pharma industry: possibilities and challenges," *Emerg. Pharm. Ind. Growth with Ind. IoT Approach*, pp. 195–216, Jan. 2020, doi: 10.1016/B978-0-12-819593-2.00007-8.

[25] M. Ficzere, O. Péterfi, A. Farkas, Z. K. Nagy, and D. L. Galata, "Image-based simultaneous particle size distribution and concentration measurement of powder blend components with deep learning and machine vision," *Eur. J. Pharm. Sci.*, vol. 191, p. 106611, Dec. 2023, doi: 10.1016/J.EJPS.2023.106611.

[26] L. A. Mészáros *et al.*, "Digital UV/VIS imaging: A rapid PAT tool for crushing strength, drug content and particle size distribution determination in tablets," *Int. J. Pharm.*, vol. 578, p. 119174, 2020.

[27] L. A. Mészáros *et al.*, "UV/VIS imaging-based PAT tool for drug particle size inspection in intact tablets supported by pattern recognition neural networks," *Int. J. Pharm.*, vol. 620, p. 121773, May 2022, doi: 10.1016/J.IJPHARM.2022.121773.

[28] L. D. Simionato, L. Petrone, M. Baldut, S. L. Bonafede, and A. I. Segall, "Comparison between the dissolution profiles of nine meloxicam tablet brands commercially available in Buenos Aires, Argentina," *Saudi Pharm. J.*, vol. 26, no. 4, pp. 578–584, May 2018, doi: 10.1016/J.JSPS.2018.01.015.

[29] N. Bolourchian, M. Nili, S. M. Foroutan, A. Mahboubi, and A. Nokhodchi, "The use of cooling and anti-solvent precipitation technique to tailor dissolution and physicochemical properties of meloxicam for better performance," *J. Drug Deliv. Sci. Technol.*, vol. 55, p. 101485, 2020.

[30] Malvern Instruments Limited, "Mastersizer S, Mastersizer 2000 and Mastersizer 3000: Method transfer-how to get the same results on all three systems," 2015.

[31] "Scaled conjugate gradient backpropagation - MATLAB trainscg." Accessed: Mar. 06, 2024. [Online]. Available: https://www.mathworks.com/help/deeplearning/ref/trainscg.html

[32] "Bayesian regularization backpropagation - MATLAB trainbr." Accessed: Feb. 26, 2024. [Online]. Available: https://www.mathworks.com/help/deeplearning/ref/trainbr.html

[33] Y. Zhang *et al.*, "DDSolver: An Add-In Program for Modeling and Comparison of Drug Dissolution Profiles," *AAPS J.*, vol. 12, no. 3, p. 263, Sep. 2010, doi: 10.1208/S12248-010-9185-1.

Highlights

- Innovative approach in dissolution prediction utilizing UV and VIS images
- VIS images enable a non-destructive prediction of compression force
- Particle size evaluation utilizing UV and VIS images for dissolution prediction
- Utilizing machine vision to gather information on API content
- Machine vision-based comprehensive quality assessment of tablets

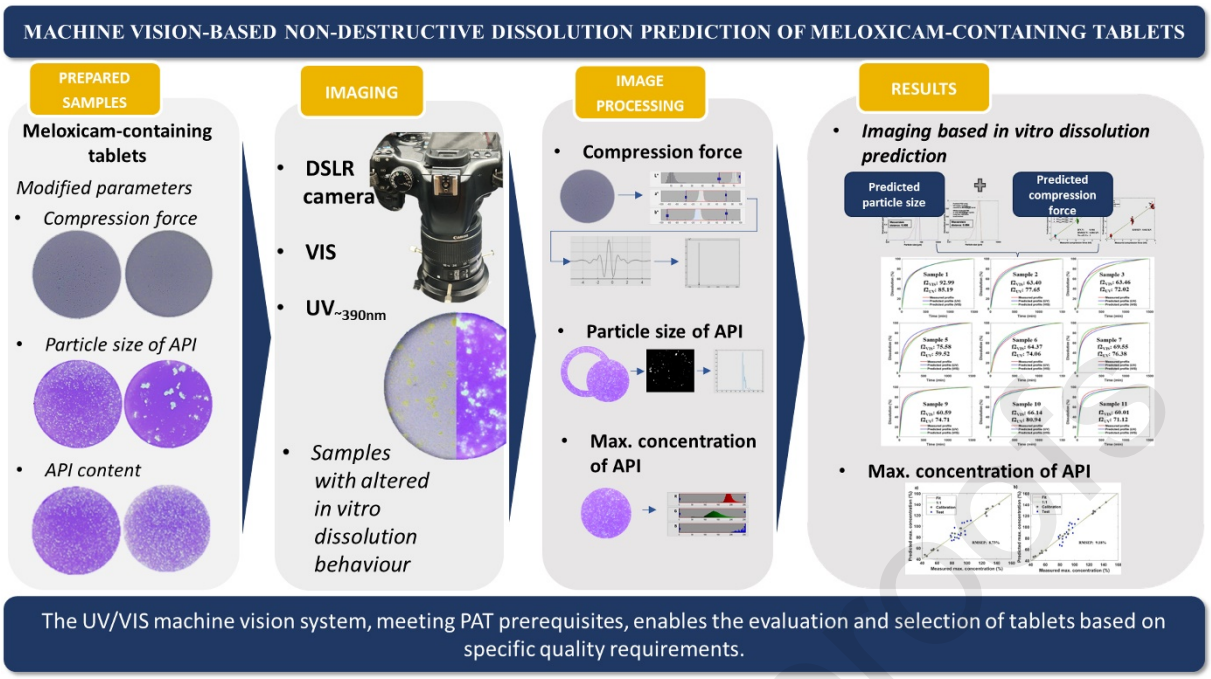

Declaration of interests

☒ The authors declare that they have no known competing financial interests or personal relationships that could have appeared to influence the work reported in this paper.

☐ The authors declare the following financial interests/personal relationships which may be considered as potential competing interests: